Int. J. Energy Res. (2017) 42, 27-52. DOI: 10.1002/er.3750

Advancements in DEMO WCLL breeding blanket design and integration

E. Martelli[b], A. Del Nevo[a], P. Arena[d], G. Bongiovì[d], G. Caruso[b], P.A. Di Maio[d], M. Eboli[c], G. Mariano[b], R. Marinari[c], F. Moro[f], R. Mozzillo[e], F. Giannetti[b], G. Di Gironimo[e], A. Tarallo[e], A. Tassone[b], R. Villari[f]

[a]*ENEA FSN-ING-PAN, ENEA CR Brasimone, Località Brasimone, 40032, Camugnano (BO), Italy*
[b]*DIAEE, Sapienza University of Rome, Corso Vittorio Emanuele II, 244, 00186, Roma, Italy*
[c] *DICI, University of Pisa, Largo Lucio Lazzarino 2, 56122, Pisa, Italy*
[d]*University of Palermo, Viale delle Scienze, Edificio 6, 90128, Palermo, Italy*
[e] *CREATE, University of Naples Federico II, DII, P.le Tecchio 80, 80125, Napoli, Italy*
[f] *ENEA FSN-FUSTEC-TEN, C.R. Frascati, via E. Fermi 45, 00044 Frascati, Italy*

The Water-cooled lithium-lead breeding blanket is a candidate option for European DEMO nuclear fusion reactor. This breeding blanket concept relies on the liquid lithium-lead as breeder-multiplier, pressurized water as coolant and Eurofer as structural material. Current design is based on DEMO 2015 specifications and represent the follow up of the design developed in 2015. The single module segment approach is employed. This is constituted by a basic geometry repeated along the poloidal direction. The power is removed by means of radial-toroidal (i.e. horizontal) water cooling tubes in the breeding zone. The lithium lead flows in radial-poloidal direction. On the back of the segment a 100 mm thick plate is in charge to withstands the loads due to normal operation and selected postulated initiating events. Water and lithium lead manifolds are designed and integrated with a consistent primary heat transport system, based on a reliable pressurized water reactor operating experience, and the lithium lead system. Rationale and features of the single module segment water-cooled lithium-lead breeding blanket design are discussed and supported by thermo-mechanics, thermo-hydraulics and neutronics analyses. Preliminary integration with the primary heat transfer system, the energy storage system and the balance of plant is briefly discussed. Open issues and areas of research and development needs are finally pointed out.

Keywords: Breeding Blanket, DEMO, WCLL

1. Introduction

In a fusion power plant, the Breeding Blanket (BB) is a key component since it has to withstand severe conditions while insuring tritium self-sufficiency, adequate neutron shielding, to remove the heat generated in the tokamak plasma and to transfer it to the Primary Heat Transfer System (PHTS) ensuring an efficient power conversion. The features of the blanket system will impact the DEMO (DEMOnstration Power Plant) [1] design, availability, safety and environmental aspects and cost of electricity.

The Water-Cooled Lithium-Lead (WCLL) BB is considered a candidate option for the European DEMO nuclear fusion reactor [2]. It relies on EUROFER as structural material, liquid Lithium-Lead (PbLi) ^{6}Li enriched at 90% as breeder, neutron multiplier and tritium carrier, and water as coolant at Pressurised Water Reactor (PWR) conditions. Design activities are pursued to develop and to deliver a feasible and integrated conceptual design of the WCLL BB in the framework of the H2020 EUROfusion Project [3].

Starting from the studies done for the WCLL BB design in 2015 [4], an advanced design, based on the single module segment approach, is developed. This configuration allows to solve some drawbacks identified in former design [4] (e.g. PbLi drainage and He removal from the breeding zone) as well as to facilitate the manifolds integration and the TBR performances.

The design features are evaluated by means of neutronic, thermo-mechanic (TM), thermo-

author's email: emanuela.martelli@uniroma1.it

hydraulic (TH) and magneto-hydrodynamic (MHD) analyses. The paper presents the results of the analyses, and finally underlines open issues and areas of research and development (R&D) needed.

2. Design: rationale and description

The WCLL BB design is based on 2015 DEMO CAD model, which is characterized by 18 sectors. Each DEMO sector (20°) is composed by two inboard segments and three outboard segments (Fig. 1). Each sector has an upper port and a lower port [5] to allow the feeding and the outlet of the water coolant and the PbLi pipelines (Fig. 2). The main geometry of the segments is simplified to face, as much as possible, manufacturing and remote handling issues.

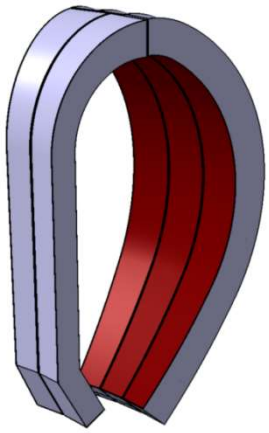

Fig. 1 WCLL BB DEMO sector

The WCLL BB version 2016 is designed with the single module segment approach with a basic breeding cell element repeated along the poloidal direction. The single BB segment is composed by the following components:

- First Wall (FW) and Side Walls (SW);
- top and bottom caps;
- internal stiffening and baffle plates;
- Back Supporting Structure (BSS);
- Breeding Zone (BZ) cooling pipes;
- Lithium Lead (PbLi) internal manifold;
- Inlet and outlet BZ cooling water manifolds;
- inlet and outlet manifolds of first wall cooling system

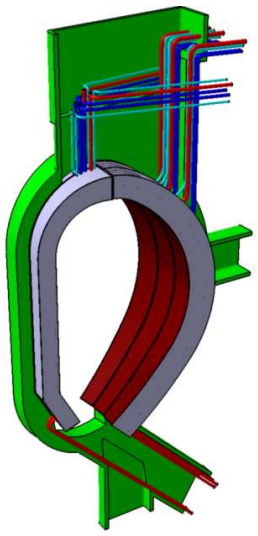

Fig. 2 DEMO sector piping system

The FW of the segment (inboard and outboard) is single curved in poloidal direction, with a thickness of 25 mm. The FW plasma facing area is covered with a tungsten layer of 2 mm thickness (red surface in Fig. 1). The FW is cooled by water flowing in square channels in counter-current direction along a radial-toroidal path (Fig. 3). The channel distance is calculated accounting for the pitch of two consecutive stiffening plates delimiting the basic breeding cell.

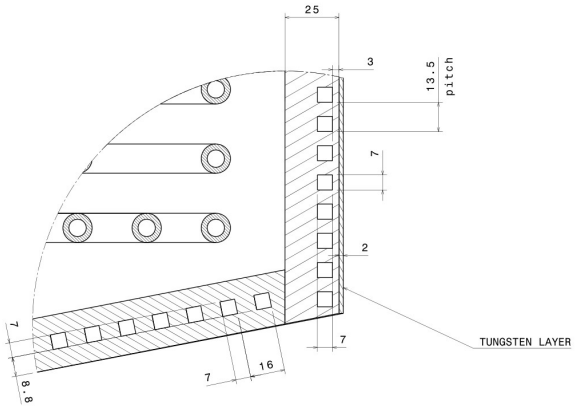

Fig. 3 Layout of FW cooling channels

In order to guarantee the structural integrity of each segments against the over pressurization, the WCLL BB segments (inboard and outboard) are equipped with internal stiffening plates placed along poloidal-radial (PR) and toroidal-radial (TR) planes. Each segment has five PR stiffening plates of 16 mm thickness and about 100 TR ribs of 12 mm thickness (Fig. 4).

The PbLi circulation is ensured by baffle plates of 2 mm thick, placed along the toroidal-radial direction. The distance between TR stiffening plates and baffle plates is 135 mm and is calculated on a curvilinear coordinate. The TR ribs and baffle plates are planar and locally normal to BB curve surface facing the plasma (Fig. 5). The FW channels are symmetrical with respect to the plane of TR and baffle plates.

The TR stiffening plates define in each BB segment about 100 radial-toroidal elementary cells. The BZ cooling tubes, placed in each cell, (Fig. 6) are double walled and have external diameter of 13.5 mm, the internal one of 8 mm and the thickness is 1.25 mm.

The BZ area for the inboard and outboard module is, respectively, 450 mm and 800 mm thick (Fig. 7).

The PbLi inlet and outlet manifolds are placed inside the segment structure, delimited by walls of 30 mm thick (Fig. 7).

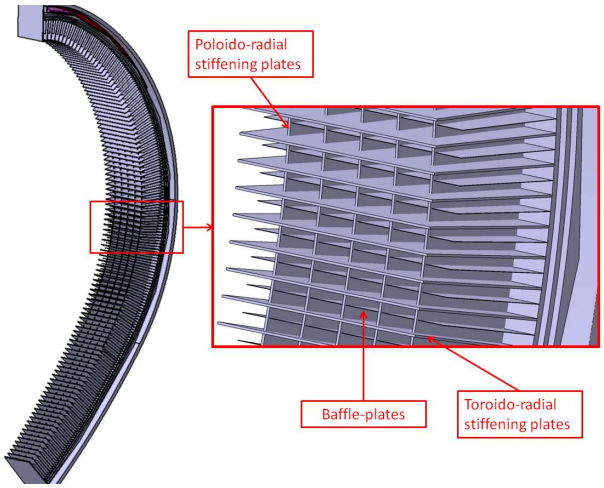

Fig. 4 WCLL BB module internal structure

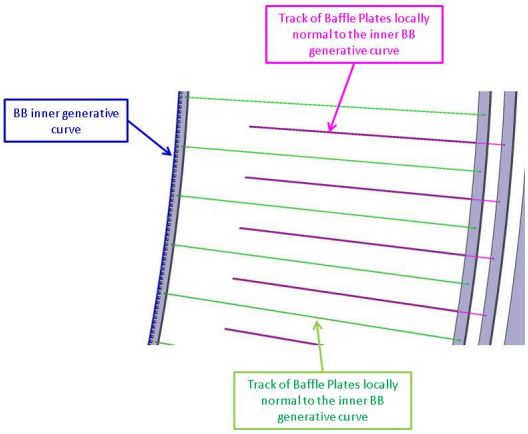

Fig. 5 Track of baffle plates and TR stiffening plates

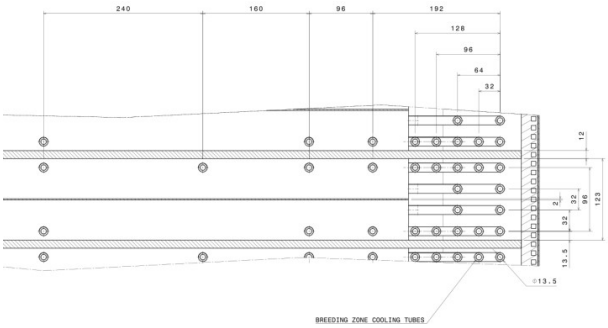

Fig. 6 Layout of BZ cooling tubes in the basic breeding cell

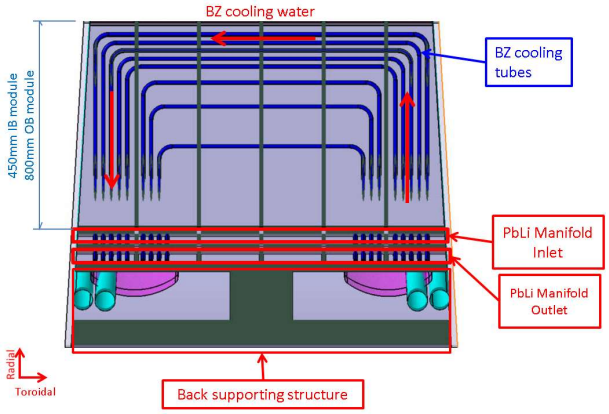

Fig. 7 Section of the single module on toroidal-radial plane

The back walls of the segments are properly cut in the back area to save space for the BZ and FW cooling water manifolds (Fig. 8 and Fig. 9).

The BSS of the segments (inboard and outboard) have T-shape and are joined to the sidewalls and the back walls of the modules (Fig. 7).

The five segments of each DEMO sector are fed by dedicated piping system. The pipes are routed through the upper and lower port of DEMO Vacuum Vessel (VV).

In particular, in the upper port are routed the following piping lines (Fig. 10) of the five BB segments:

- FW water inlet and outlet
- BZ water inlet and outlet
- PbLi inlet

The lower port contains only the PbLi outlet pipes, as shown in Fig. 11.

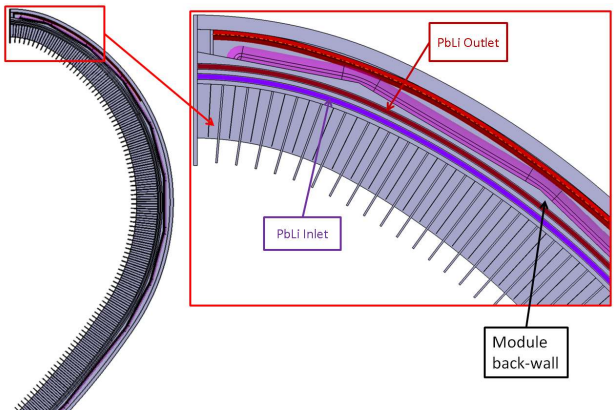

Fig. 8 Back-wall and PbLi manifold region

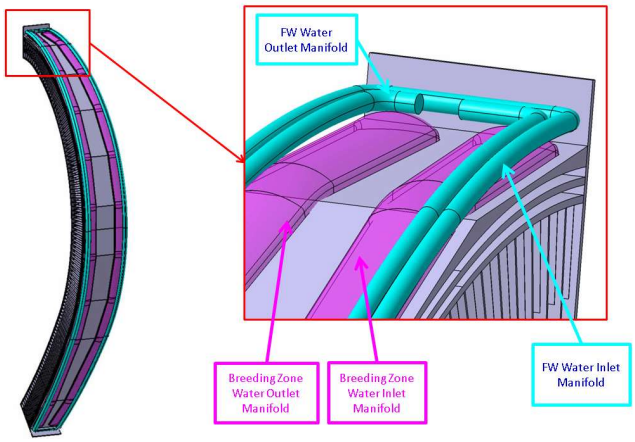

Fig. 9 BZ and FW cooling water manifold

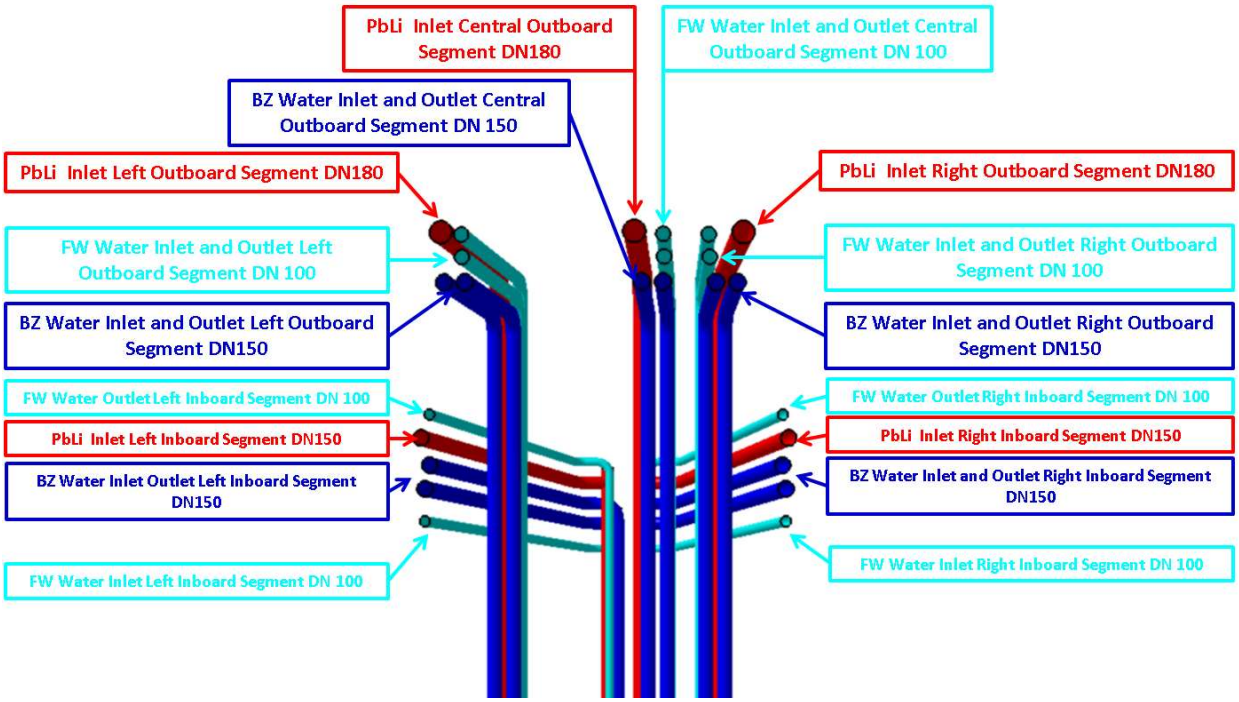

Fig. 10 Layout of WCLL BB feeding pipes in the upper port

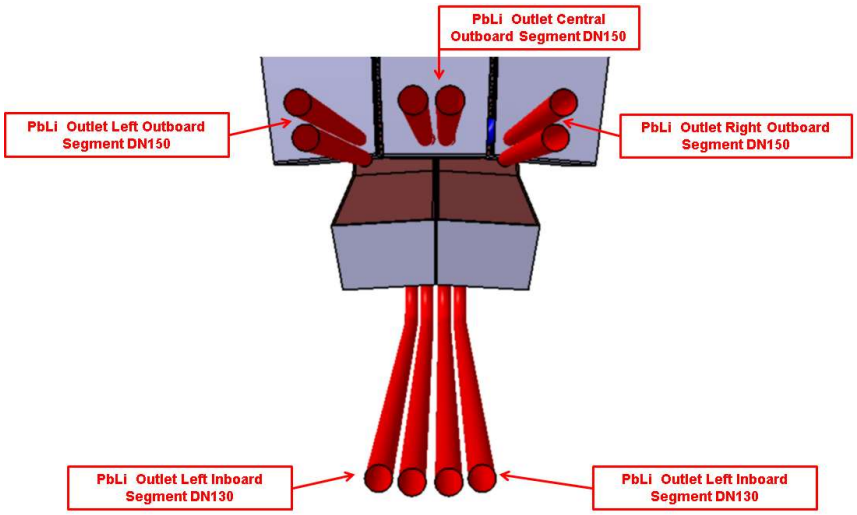

Fig. 11 Layout of WCLL BB feeding pipes in the lower port

3. Neutronic analyses

The neutronic analyses of the DEMO WCLL breeding blanket are aimed at the evaluation of the nuclear performances of the design concept. Three dimensional coupled neutron and gamma transport simulations are performed using the MCNP5v1.6 Monte Carlo code [6] and JEFF 3.2 [7] nuclear data libraries in order to assess tritium self-sufficiency, shielding capabilities of the breeding blanket/manifold system, as well as the spatial distribution of the neutron flux, nuclear heating, neutron damage and he-production according to specific guidelines [8].
The WCLL DEMO MCNP model with homogenous blanket modules [9] is based on the 2015 DEMO1 baseline configuration, which plasma parameters are shown in Table 1: it represents a 10° toroidal sector of the tokamak, including Toroidal Field Coils (TFC), VV, Divertor, blanket segmented boxes, ports, and plasma chamber.

Table 1. Plasma parameters of the DEMO 2015 baseline configuration

Major radius (m)	9.072
Minor radius (m)	2.927
Aspect ratio	3.1
Plasma elongation	1.59
Plasma triangularity	0.33
Fusion power (MW)	2037

The WCLL MCNP DEMO model has been further implemented integrating the detailed WCLL breeding blanket structure and updated manifold materials according with the design features of the version 2016. It should be noted that the analyses have been carried out keeping the multi module approach, as in the 2015 WCLL conceptual design, to compare the results with the analyses performed in 2015. Indeed, the enhanced breeding performances of the single module segment approach are expected, predictable and currently out of the scope of the analyses.

3.1 WCLL DEMO MCNP model

The CAD model of the WCLL Outboard #4 blanket module has been preprocessed and properly simplified by means of the 3D modeling software Ansys SpaceClaim 2015 [10] to generate a model suitable for neutronic analyses. A single breeding unit (e.g. the components included between two neighboring stiffening plates, red area in Fig. 12) has been isolated and singularly converted into the equivalent MCNP geometry through the CAD-to-MCNP interface MCAM (SuperMC_MCAM5.2 [11]).

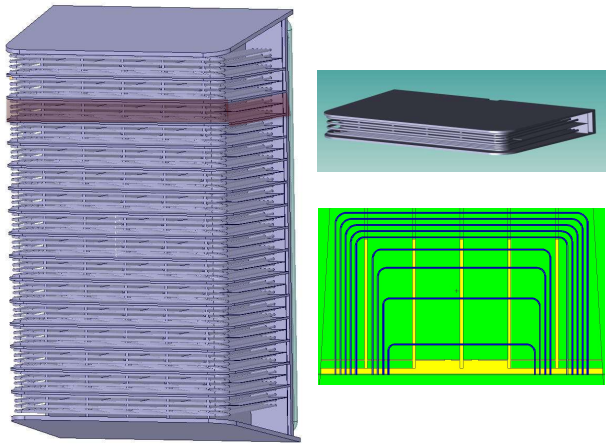

Fig. 12 WCLL blanket module: breeding unit inside the blanket model (left panel) and isolated (top right) and a section of the equivalent MCNP model along the cooling pipes axis

Then, the single breeding unit is recursively integrated filling the DEMO MCNP generic model inboard and outboard (full and halved) blanket modules #4: as far as the inboard module integration is concerned, the driving criterion, chosen to take into consideration its reduced radial extension, is the maintenance of the distance between the FW and the outermost cooling channel (Fig. 13).
The other blanket modules, as well as the back supporting structure and manifolds have been represented developing specific homogenized compounds with volume percentages of the materials (EUROFER, H_20, PbLi) extracted by the engineering CAD files.

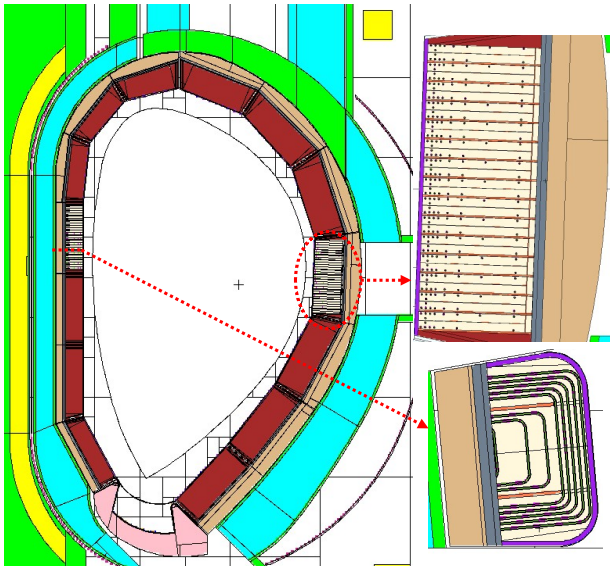

Fig. 13 WCLL DEMO MCNP model integrating detailed blanket in the Inboard and Outboard #4 blanket modules

3.2 Nuclear Analyses

The model described is used to evaluate the performances of the WCLL DEMO in term of shielding capability, i.e. TFCs irradiation damage reduction, and tritium self-sufficiency. The neutron flux, nuclear heating, damage and He-production radial profile are assessed on the equatorial mid plane, thus considering the detailed description of the breeding blanket structure.

The global Tritium Breeding Ratio (TBR) for the analyzed WCLL DEMO configuration is 1.14 and, thus, it guarantees the self-sufficiency of the reactor. The 99.7% of the tritium is produced in the breeding area, the remaining fraction is generated in the back supporting structure where the inlet PbLi inlet pipes are located. A comparison between the TBR produced in the Outboard blanket module #4 and the corresponding values obtained using homogenized material highlights a gain in the TBR of about 5% due to the detailed description of the blanket. Applying this correction factor to the total TBR a predictable value of about 1.20 can be estimated: this evaluation must be confirmed through the calculation performed on a full detailed WCLL DEMO.

Neutron flux, nuclear heating, dpa and He-production in steel components have been calculated along the inboard mid-plane.

The total and fast (E>100 KeV) neutron fluxes (Fig. 14) at the FW are respectively $5x10^{14}$ n/cm^{2}s and $3.4x10^{14}$ n/cm^{2}s; the blanket/manifold system provides an attenuation of more than two orders of magnitude to the VV inner shell. The neutron flux further decreases by several orders of magnitudes across the VV, being $4.8x10^{8}$ n/cm^{2}s (total) and $2.9x10^{8}$ n/cm^{2}s(fast) on the TFCs, well below the 10^{9} n/cm^{2}s threshold limit.

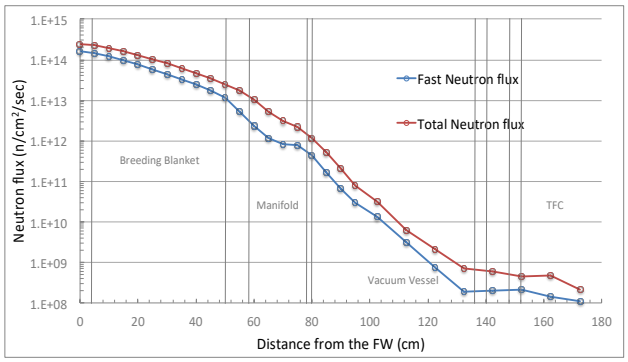

Fig. 14 Radial profile of the neutron flux evaluated in the inboard equatorial plane

The maximum values of the nuclear heating on steel components (Fig. 15) are ~7.5 W/cm^3 on FW EUROFER and 0.1 W/cm^3 on the VV inner shell. In the TFC winding pack the heat load density is $1.4x10^{-5}$ W/cm^3, satisfying the design limit of 50 W/m^3.

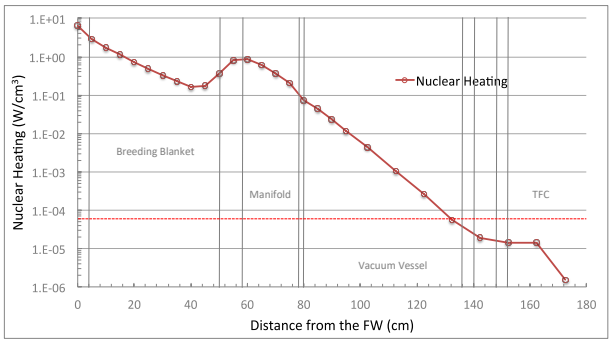

Fig. 15 Radial profile of the nuclear heating on Eurofer evaluated in the inboard equatorial plane

Fig. 16 shows the Inboard radial profile of the damage on EUROFER and SS-316: the 9.8 dpa/FPY value assessed at the FW decreases to ~$6.2x10^{-3}$ at the VV. Considering the limit of 2.74 dpa foreseen on the VV steel, the present configuration ensures a sufficient protection over the whole DEMO lifetime.

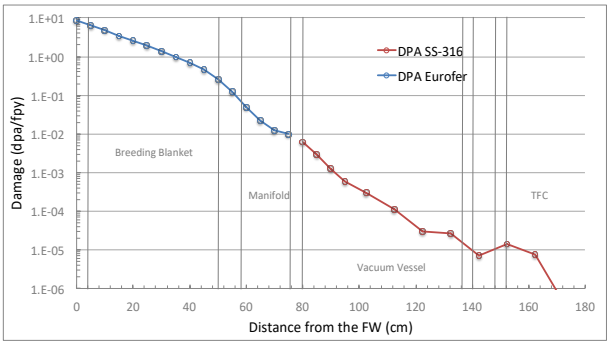

Fig. 16 Radial profile of the damage on Eurofer (up to the manifolds) and SS-316, evaluated in the Inboard equatorial plane

Regarding the He-production in steel (Fig. 17), the estimation performed highlights a reduction of about 2 orders of magnitude from the FW (100 appm/FPY) to the VV (1 appm/FPY). Behind the VV the He-production drops to values below 10^{-4} appm/FPY.

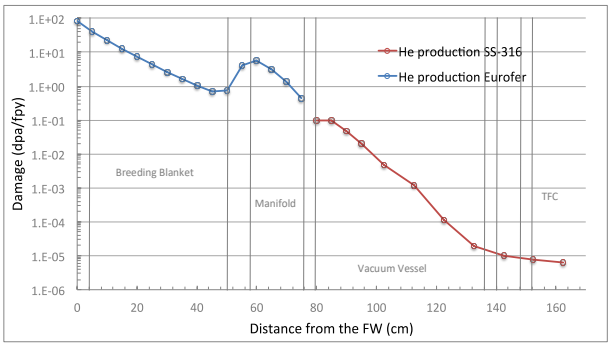

Fig. 17 Radial profile of the He-production on Eurofer (up to then manifolds) and SS-316 evaluated in the Inboard equatorial plane

The results of the nuclear analyses, performed on the WCLL DEMO integrating the recent blanket design, highlighted that the tritium self-sufficiency design target and shielding requirements aimed at the protection of the VV and toroidal superconductive coils are fulfilled. A further enhancement of the blanket/manifold system performances must be expected with the development of the new 'banana' concept of the breeding blanket, both in terms of tritium production and in shielding effectiveness.

4. Thermo-hydraulic analyses

4.1 BZ analyses

Thermo-hydraulic analyses of the breeding zone have been performed to verify the efficiency and optimize the design of the cooling system, ensuring that the temperature requirement of the structures is met.

A CFD model of the basic breeding cell is developed to obtain a complete and detailed temperature distribution. The analyses are executed through ANSYS workbench exploiting CFX solver (ver. 15.0).

The basic breeding cell has a total height of 135 mm and it is divided in 6 channels in toroidal direction; a baffle plate at mid-plane defines the PbLi flow path in radial-poloidal direction. It includes 21 coolant double wall tubes (DWT), with an internal diameter of 8 mm. The FW coolant system is characterized by 10 square channels of 7 mm.

The CFD model, Fig. 18, includes solid domains (i.e. stiffening plates, tubes, FW structure and tungsten layer) and fluid domains (i.e. PbLi, BZ and FW water coolant).

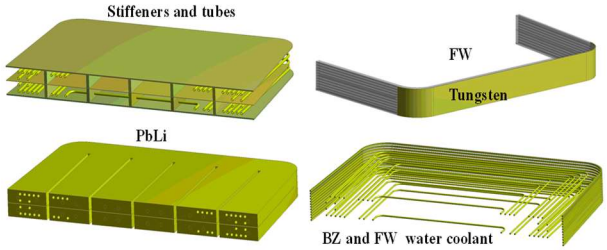

Fig. 18 CFD solid and fluid domains

The mesh model is characterized by hexahedral and tetrahedral elements. Considering the geometrical features of the domains, many local controls are inserted to define appropriately the complex geometry. Despite the complexity, a satisfactory result is achieved in terms of quality of the mesh. Fig. 19 reports a radial-poloidal section of the mesh.

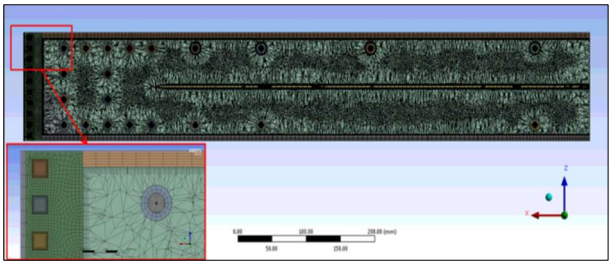

Fig. 19 CFD mesh

The reference calculation is set up evaluating the power in the FW and in the BZ, and calculating through the enthalpy balance the

water coolant mass flow rates. For a total power of 3.46 MW in the elementary breeding cell (see Table 2), the total mass flow rate is 1.529 kg/s, divided in 0.562 kg/s in the FW and 0.967 kg/s in the BZ. The results of simulations are summarized in Table 3.

Table 2. CFD boundary conditions

	Case 0	Case 1	Case 2
Total Power [MW]	3.46	3.46	3.46
FW [MW]	1.27	1.27	1.27
BZ [MW	2.19	2.19	2.19
Total Mflow[kg/s]	1.529	1.529	1.529
FW	0.562	0.676	0.562
BZ	0.967	0.881	0.967
FW/BZ T inlet [°C]	285	285	285
PbLi mass flow rate [kg/s]	0.14	0.14	0.14
PbLi T inlet [°C]	325	325	325

Table 3. CFD results

	Case 0	Case 1	Case 2
Ave. Vout [m/s]			
FW	1.76	2.06	1.73
BZ	1.40	1.28	2.78
Ave. Tout [°C]			
FW	329	324	326
BZ	322	325	331
PbLi Ave. Vout [m/s]	0.002	0.002	0.002
PbLi Ave. Tout [°C]	330.8	324.7	328.6

The results demonstrate that the FW coolant system extracts a part of the power deposited in the BZ, as the FW average outlet temperature (329 °C) is higher than the expected value of 325 °C and, conversely, the BZ average outlet temperature is lower (322 °C). The BZ water bulk temperature, reported in Fig. 20, is calculated for groups of tubes, according to radial displacement in the elementary cell and temperature distribution (i.e. Group 1 and 2 include tubes near the FW, Group 3 and 4 include central tubes and Group 5 includes tubes near the BP). The maximum average temperature is 330 °C, which is lower than the saturation temperature (saturation temperature is 344 °C at 15.5 MPa). Fig. 21 shows the FW average bulk temperature, presenting a maximum value of 338 °C.

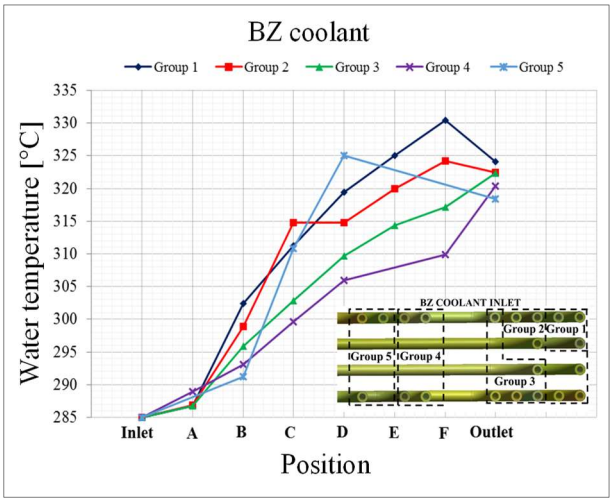

Fig. 20 CFD results, Case 0 BZ coolant bulk temperature

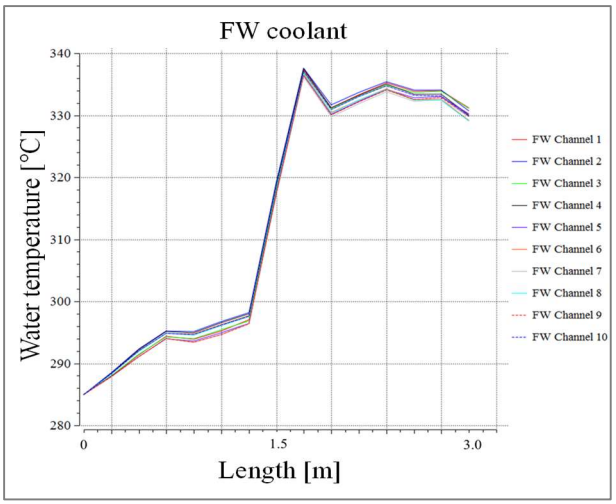

Fig. 21 CFD results, Case 0 FW coolant temperature

Starting from the results of thermo-mechanical analyses [12], a calculation (Case 1) is carried out assuming different mass flow rates in BZ tubes. The FW mass flow rate is increased (0.676 kg/s) and the BZ mass flow rate is decreased (0.8807 kg/s), with respect to the previous case. As regard the BZ and FW thermal fields, it is noted that the FW outlet temperature is decreased (324 °C) with respect to the reference case and the BZ temperature is increased (325 °C), presenting a homogeneous outlet temperature distribution. Fig. 22 and Fig. 23 present the coolant bulk temperature in the FW and BZ system, respectively. The maximum bulk temperature is about 330 °C in the FW and 328 °C in the BZ.

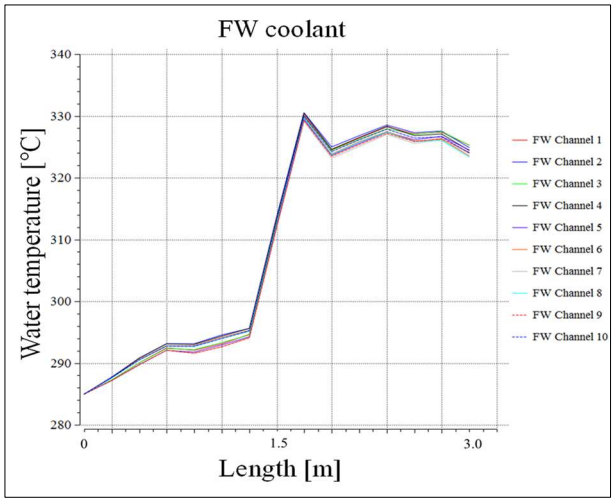

Fig. 22 CFD results, Case 1 FW coolant Temperature

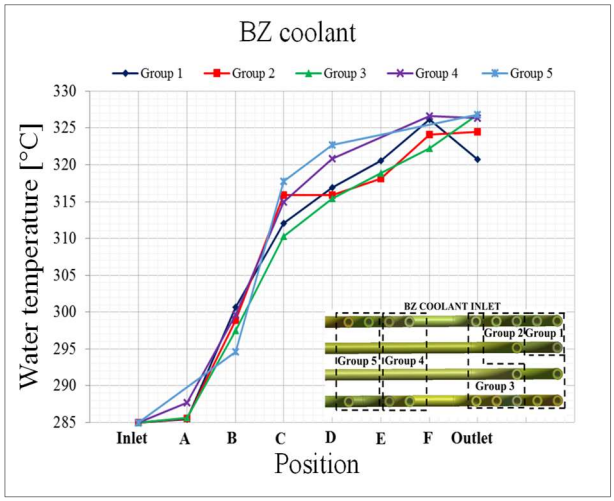

Fig. 23 CFD results, Case 1 BZ coolant temperature

The BZ and FW average outlet velocities are in the range between 1.3 m/s and 2.0 m/s and, being below the required limit (7 m/s), it is possible to improve the coolant efficiency.

Comparing the two simulations, it is observed that the stiffeners temperature is not affected by the coolant mass flow distribution. The maximum temperature (415 °C) in the solid structures (i.e. EUROFER) is far from the limit (i.e. 550 °C) in both cases. The thermal field of the stiffeners calculated in the Case 0 is reported in Fig. 24a.

The stiffeners and PbLi domains present an asymmetric thermal field in toroidal direction, due to the BZ water layout. The asymmetry is an issue, since it is a source of thermal stress for the EUROFER structures. Moreover, the toroidal asymmetry determines the presence of two regions with different PbLi density and, due to the buoyancy forces, a net flow in the toroidal direction in addition to the dominant radial-poloidal flow (see Fig. 24b).

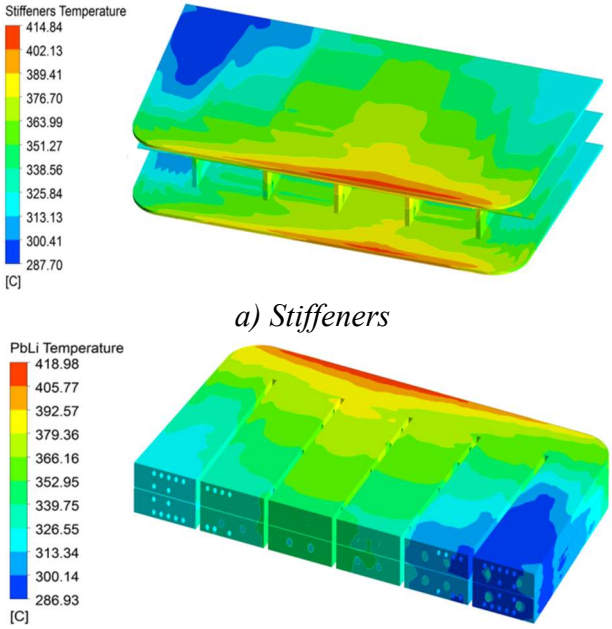

a) Stiffeners

b) PbLi

Fig. 24 CFD results, Case 0 stiffeners and PbLi temperature

To achieve a symmetric temperature distribution, a new BZ coolant layout has been investigated (Case 2). In this case the BZ water mass flow rate enters in the 10 tubes nearby the FW, then it recirculates in the other 11 tubes. The schematization of BZ coolant inlet and outlet is reported in Fig. 25.

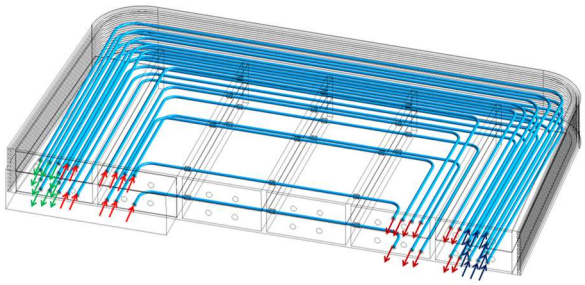

Fig. 25 CFD analysis: Case 2 BZ scheme

The results confirmed that, by recirculating the BZ water coolant, a symmetric thermal field of PbLi and stiffeners can be achieved (see Fig. 26). Moreover, a more uniform distribution of PbLi outlet mass flow rate was evidenced. Regarding the BZ coolant system, the average outlet velocity is increased (2.78 m/s), with an

outlet temperature of 331 °C, which is higher than the expected value. Further analyses will be performed to investigate this configuration, optimizing the coolant systems efficiency.

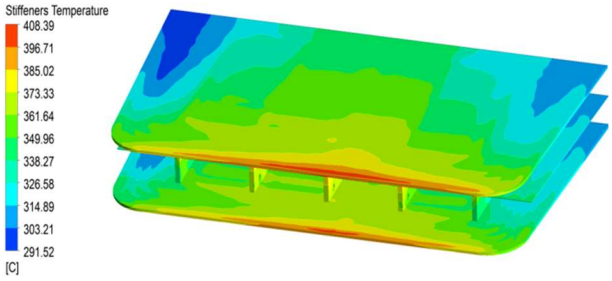

a) Stiffeners

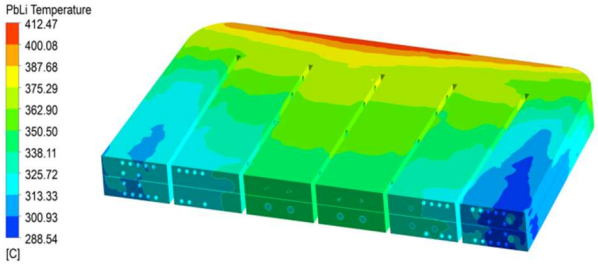

b) PbLi

Fig. 26 CFD results, Case 2 stiffeners and PbLi temperature.

4.2 MHD analysis

The interaction between the tokamak magnetic field and the PbLi in the WCLL module causes the transition of the flow regime from the ordinary hydrodynamic behavior to the magnetohydrodynamic (MHD) one. A MHD flow is characterized by the coupling between the velocity and the magnetic field: currents are induced inside the electric conductive fluid, which cause the arising of Lorentz forces that dampen the mean velocity, suppress the turbulence structures not aligned with the magnetic field and, more in general, greatly modify the flow features [13]. The design of a breeding blanket for a tokamak reactor like DEMO cannot overlook to address these issues.

A pioneering CFD analysis was performed to identify the main features of the MHD flow inside the elementary cell of the WCLL module and to provide an estimate of the additional pressure drop due to the electromagnetic drag in the BZ. The MHD pressure drop is one of the main concerns for the blanket design, since it can exceed the hydrodynamic term by several orders of magnitude.

The fundamental governing parameters for a MHD flow are the Hartmann number (M), which is proportional to the magnetic induction intensity and the fluid electric conductivity, and the wall conductance ratio (c), which measures how much the walls bounding the flow are conductive compared to the fluid. For a fusion blanket like the WCLL, the value of M can reach values up to 10^4.

Since no mature computational MHD code is currently available, the commercial ANSYS CFX was employed instead to perform the analysis. The MHD solver of CFX is based on the induction-less approximation that assumes the applied magnetic field as determined only by the boundary conditions.

A preliminary validation of the software was carried out to assess its capability to properly represent basic 2D MHD flows for natural and forced convection, following the guidelines exposed by Smolentsev [14] and Di Piazza & Buhler [15]. An excellent agreement with reference results was found up to $M = 10^3$ for the limiting case of perfectly conducting ($c = \infty$) and insulating walls ($c = 0$). An overview of the benchmark results is available in Table 4.

The elementary cell of the equatorial outboard module was considered in the analysis focusing on the central channel. The fundamental parameters of the WCLL cell are available in Table 5. The model geometry was simplified removing both FWs and DTWs, as well as extending the radial-poloidal stiffening plates (SP) to connect them to the first wall. These additional dummy walls were employed to prevent cross-flows toward the nearby channels, which were not modelled, and were assumed to have the same electric conductivity of the fluid. For a sketch of the simulation geometry, see Fig. 27.

The PbLi flow was considered as isothermal at 600 K. The fluid thermo-physical properties at this temperature were evaluated with the relations reported by de les Valls [16] and added to the CFX libraries. The solid domain was modeled as EUROFER steel at the same reference temperature with properties calculated according to Mergia & Boukos [17].

The velocity profile at the inlet was assumed to be fully developed and with a conservative value of the mean velocity (1.5 mm/s, as opposed to the maximum velocity of 0.25 mm/s considered in section 4.1), whereas a zero-pressure boundary condition was assumed at the outlet. The flow is laminar. Electric current density and potential were conserved at the fluid/solid interface, whereas at the external surfaces of the solid domain a boundary condition of zero-current for the normal component was employed.

Table 4 Validation results for peak (p.e.) and integral error (i.e.)

Buoyant test case				P-driven test case			
c	***M***	**p.e.[%]**	**i.e.[%]**	**c**	***M***	**p.e.[%]**	**i.e.[%]**
0	10^2	0.68	n.a.	0	$5{\cdot}10^2$	n.a.	0.54
	$4{\cdot}10^2$	4.08			$5{\cdot}10^3$		0.21
	10^3	2.08			10^4		0.01
					$1.5{\cdot}10^4$		0.44
∞	10^2	2.01	0.79	∞	10^2	2.85	0.03
	$4{\cdot}10^2$	1.26	1.49		$4{\cdot}10^2$	3.08	0.14
	10^3	2.20	1.46		10^3	7.14	0.13

Table 5 WCLL parameters. L and H are half-lengths, in brackets are reported the values of M used in the simulation

Dimensionless groups				Geometry parameters	
	c	***M***	**Re**		**[mm]**
Baffle	$1.25{\cdot}10^{-2}$	$9.8{\cdot}10^3$	$7.87{\cdot}10^2$	**L(toroidal)**	117
SP(toroidal)	$7.50{\cdot}10^{-2}$	$(4.9 \div 9.8 \cdot 10^2)$		**H(poloidal)**	33.1
SP(poloidal)	$10.0{\cdot}10^{-2}$			**Z(radial)**	800

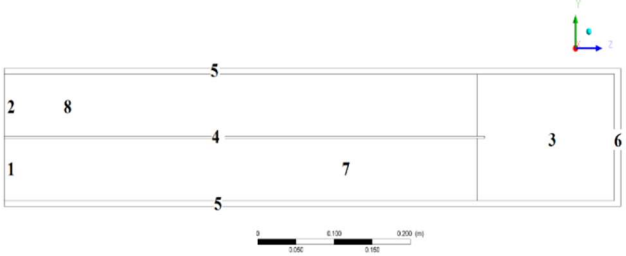

Fig. 27 WCLL MHD analysis computational domain. Fluid: 1) inlet, 2) outlet, 3) bend, 7) inlet duct, 8) outlet duct; Solid: 4) baffle, 5) radial-poloidal SPs, 6) FW

The components in the toroidal and poloidal directions of the applied magnetic field were considered constant and uniform. The resulting magnetic induction vector has an angle $\alpha = 16°$ on the toroidal direction. Since CFX can solve reliably MHD flows in 3D geometries only for $M \leq 10^3$, the intensity of the magnetic field was scaled down to keep the simulation in this range. A non-null normal component of the magnetic field was present in every wall and thus boundary layers of thickness $\delta = L/M$ were considered.

In Fig. 28, the velocity and electric potential contour of the fully developed flow at the inlet for $M = 9.82 \cdot 10^2$ are depicted, whereas the same results for the whole cell are shown in Fig. 29. Since the toroidal component of the magnetic field is dominant ($B_t \approx 4\ B_p$), the associated normal component for the poloidal-radial SPs is higher than the one for the toroidal-radial SP and the baffle. If the magnetic field was purely toroidal, these walls would be aligned with the magnetic field and the region close to them would be characterized by jets whereas the rest of the duct would be occupied by a slug flow (core region). However, in the analyzed case, the poloidal field breaks the alignment and the jets partially detach from the walls, perturbing the core: an internal layer is created, which is oriented with the magnetic field direction. The layer separates two core regions where the slug flow is still present.

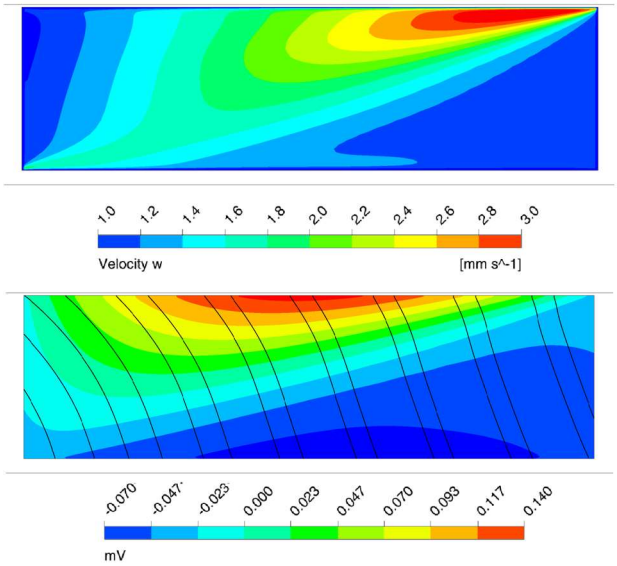

Fig. 28 Velocity (top) and electric potential contour with current paths (bottom) for the inlet duct at M = 9.82 ·10^2

Since $c \gg M^{-1}$, the duct walls are conductive and the current paths close through them. Therefore, their thickness plays an important influence on the definition of the flow features. The low value of the conductance ratio for the baffle causes the formation of a region of low electromagnetic drag close to it and the enhancement of the associated jet. The opposite happens close to the toroidal-radial SP, where the jet is suppressed because of the low resistivity path offered by the wall to the closure of the induced currents.

In the bend, the fluid is mostly stagnant. This scenario would change in the real module, where the presence of the coolant pipes and the arising of buoyant forces due to the neutronic power deposition modify the flow behavior. The axial potential difference in the bend drives currents to close through the first walls but no relevant 3D MHD effects are observed due to the combined action of the intense magnetic field, the conductive walls and the low mean velocity of the fluid. After the bend, the flow field quickly restores the fully developed state and the contours of velocity and potential in the outlet duct are the mirrored versions of those presented in Fig. 29.

For a laminar pressure-driven 2D MHD flow in a rectangular duct for $M \gg 1$, the core region is inviscid and the Lorentz force balances the pressure gradient. The value of the latter is function of the intensity of the induced currents, which in turn, since $1 \gg c \gg M^{-1}$, close through the walls and are dependent by the wall conductance ratio. The pressure gradient value can be estimated by $\Delta p/\Delta x \approx \sigma_w U_0 B_0^2 t_w/L$, where σ_w and t_w are the wall conductivity and thickness. The additional term due to 3D MHD effects is negligible in this configuration for the reasons already discussed and its incidence on the total pressure drop further decreases with the Hartmann number. Therefore, the pressure drop in the cell for an increasing value of M scale with B_0^2. This behavior is confirmed by the results of the simulations performed for M = 4.9 ÷ 9.8 ·10^2, which are plotted against M in Fig. 30.

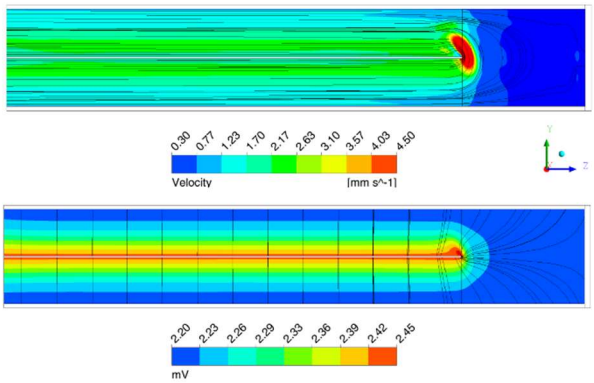

Fig. 29 Velocity contour and streamlines (top), electric potential contour with current paths (bottom) for the whole cell at M = 9.82 ·10^2

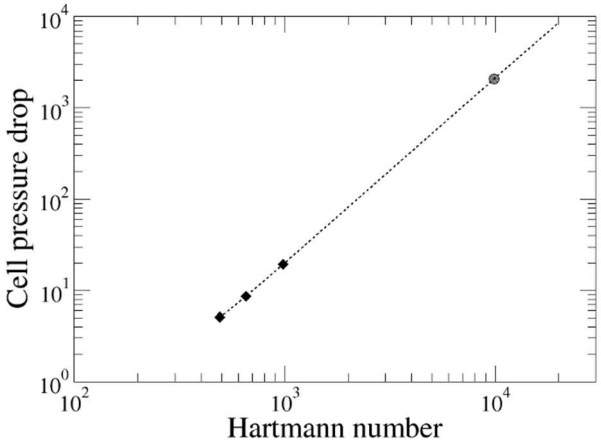

Fig. 30 Plot of cell pressure drop (in Pa) with increasing Hartmann number. Black diamonds mark simulation results with the dashed line showing the $\Delta p \propto B_0^2$ correlation. Estimation at M = 9.82 ·10^3 marked by the circle.

The pressure drop due to MHD effects in the WCLL elementary cell is estimated equal to

$2.06 \cdot 10^3$ Pa. Otherwise, the same flow without any magnetic field applied exhibits a pressure drop of $5 \cdot 10^{-2}$ Pa. Although the pressure drop increment in the cell due to the electromagnetic drag is consistent, the analysis results confirm that flow channel inserts (FCI) are not required to decouple the fluid region and the duct walls in the BZ.

Preliminary results from a more realistic study, which models the influence of the coolant pipes on the liquid metal flow, bring further support to this conclusion since 3D MHD effects due to the cross-section variations do not contribute significantly to the cell pressure drop.

For the future, a more complete analysis is envisioned, with the inclusion of the heat transfer and the extension of the computational domain to the manifold region, where most of MHD pressure drops should occur.

4.3. Thermal analysis of BSS

Thermal analyses of inboard and outboard segment BSS have been carried out to investigate the thermal behavior without cooling. Furthermore, possible cooling solutions are studied for inboard BSS.

In the CFD simulations, performed trough CFX solver of ANSYS Workbench, it is assumed the heat exchanger in a blackbody cavity with back and front temperatures of 200 °C and front temperature of 300 °C, respectively, and emissivity equals to 0.4. A radial-poloidal volumetric power density, calculated on the basis of the results of neutronic analyses and scaled with the neutron wall loads, is assigned to the inboard and outboard BSS.

The results of the outboard BSS thermal analysis demonstrate that the temperature is below the limit (550 °C) without cooling. Sensitivity analyses were performed with volumetric power density increased up to 100% of calculated values, showing a maximum temperature of 334.4 °C.

As regard to the inboard BSS, the results of the preliminary analysis show a maximum temperature of 512.2 °C, reached at top plane where the thickness is greater. Several CFD calculations are performed to investigate cooling solutions of the BSS. Fig. 31 shows the results of the inboard BSS when the front surface is cooled by water, maintaining the temperature at 300 °C. In this case the maximum temperature is 368.9 °C. Thus, further analyses should be performed on inboard BSS to optimize the cooling efficiency.

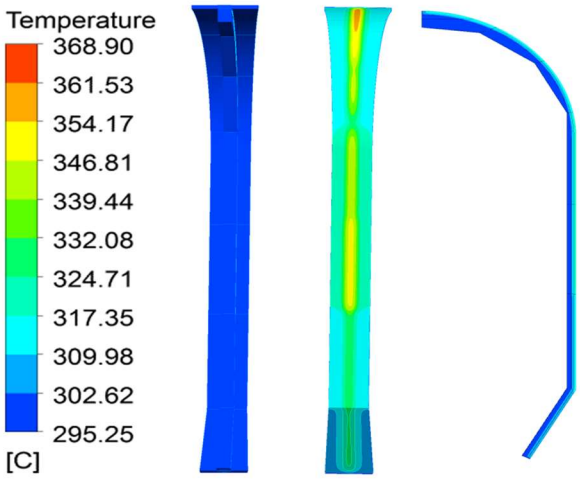

a) Inboard segment BSS

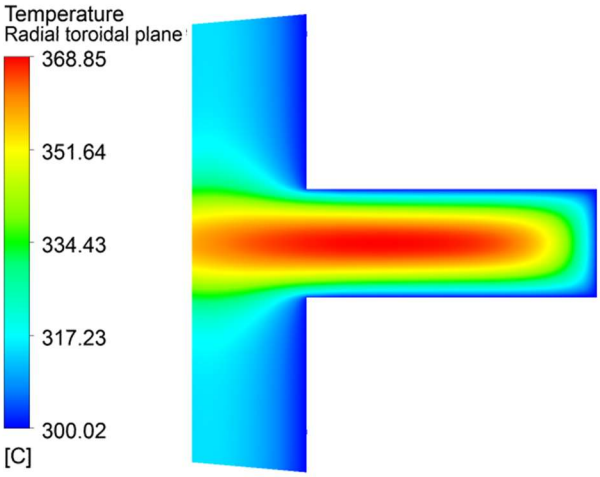

b) Radial-toroidal section at top

Fig. 31 CFD results, inboard BSS temperature with cooling

5. Thermo-mechanical analyses

Thermo-mechanical analyses are performed [19][21] to define and to qualify the DEMO WCLL BB conceptual design.

In particular, specific parametric analyses are carried out to separately assess FW and SPs thermo-mechanical performances under selected steady state loading scenarios.

Once selected the most promising FW and SPs geometric configurations, the thermo-mechanical performances of the WCLL BB equatorial outboard module (EOM) are properly investigated under both steady state nominal and accidental loading conditions

envisaged for the DEMO WCLL BB. Results obtained have allowed to identify further design modifications in order to totally accomplish the foreseen design requirements.
The research activity is performed following a theoretical-numerical approach, based on the finite element method (FEM) and adopting the qualified commercial ABAQUS FEM code.
It should be noted that the analyses discussed are based on the WCLL BB 2015 configuration, the results achieved are extended to the single module approach, with the appropriate modifications.

5.1 The FW design

The analysis has been specifically intended to optimize the FW geometric configuration, maximizing the heat flux it might safely withstand while fulfilling all the prescribed thermal-hydraulic and thermo-mechanical requirements [21]. Moreover, from the thermo-mechanical point of view, it has been assumed that the FW optimized configuration has to safely withstand the loads it undergoes under both steady state Normal Operation (NO) and Over-Pressurization (OP) loading scenarios, ensuring the fulfilment of the pertinent SDC-IC design criteria [22][23].
The FW geometric parameters potentially affecting its thermal-hydraulic and thermo-mechanical performances have been identified in the following ones (Fig. 32), and for each of them a proper range of values has been defined:

- cooling channel pitch (P) in the range 16÷26 mm;
- cooling channel width (d_c) in the range 6÷12 mm;
- cooling channel thickness (a) in the range 1÷3 mm;
- FW thickness (D) in the range 19÷25 mm.

Opportunely combining the parameter values, a set of 5929 different flat FW configurations have been considered and the thermo-mechanical performances of each one of them have been investigated when subjected to 26 different heat flux values (Φ) equally spaced in the range 0.5÷3 MW/m^2, for an overall number of 154154 parametric thermal analyses. The parametric analysis procedure has been totally automated by means of purposely set-up Python script files.

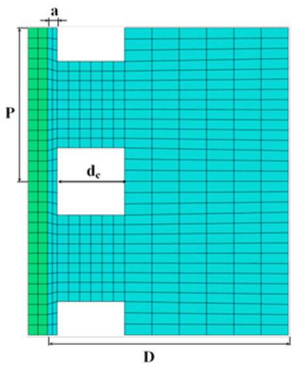

Fig. 32. FW characteristic geometric parameters.

A simplified 3D FEM model, not including breeder, Double Walled Tubes (DWTs) and coolant, has been set-up for each FW configuration considered, reproducing a toroidal-radial slice of the WCLL BB EOM, extending for two cooling channel pitches (2P) in the poloidal direction, for a breeder cell in the toroidal direction and for the whole module depth, up to the back-plate (BP), in the radial direction (Fig. 33).

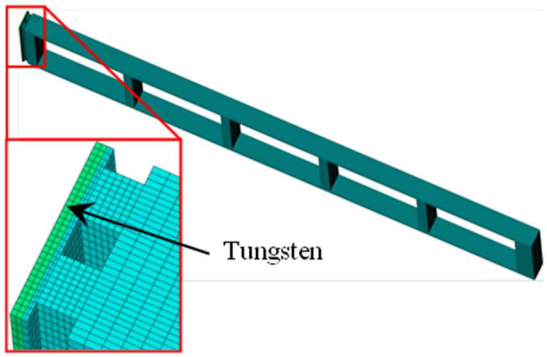

Fig. 33. Typical 3D FEM model for the FW optimization.

Thermo-mechanical loads and boundary conditions have been properly adopted in order to simulate the NO and OP steady state loading scenarios [21].
In the first step of the campaign of analysis the results of the previously mentioned 154154 steady state thermal FEM analyses have been processed in order to check the fulfilment of the prescribed FW thermal-hydraulic requirements [22] and exclude all those thermal

cases and configurations in which these requirements would have not been fulfilled. Only 66443 thermal cases have passed this first phase and, for each of them, a corresponding mechanical analysis under both NO and OP loading scenarios has been performed within the second step of the procedure. Mechanical results have been processed allowing the selection of 4 FW optimized configurations, reported in Table 6, that are able to fulfil the adopted SDC-IC design criteria (Level A and level D) up to a maximum Φ value of 2 MW/m^2.

Table 6. FW optimized configurations.

	FW 1	FW 2	FW 3	FW 4
d_c [mm]	7	7	7	7
P [mm]	16	16	16	16
a [mm]	1.0	1.0	1.0	1.0
D [mm]	22	23	24	25
Channels	93	93	93	93
u [m/s]	6.43	6.43	6.43	6.43
T_{Max} [°C]	496.8	497.0	496.9	497.0

In order to verify the outcomes of the parametric analysis, the thermo-mechanical performances of the 4 optimized configurations selected have been investigated by running more detailed and accurate FEM analyses. To this purpose, 4 different 3D FEM models have been set-up, realistically reproducing the central poloidal-radial slice of the WCLL BB EOM [20][22]. Each model includes one breeder cell in the toroidal direction and all the five breeder cells in the radial direction (Fig. 34). Moreover, Pb-Li breeder, DWTs and water flow domain have been modelled too.

Uncoupled thermo-mechanical steady state analyses have been carried out in order to assess the potential aptitude of the 4 FW optimized configurations to safely withstand the loads they undergo under NO and OP loading scenarios according to SDC-IC safety code [21].

Thermo-mechanical results have highlighted that FW 4 configuration shows the most encouraging behaviour.

From the thermal standpoint, EUROFER limit temperature of 550 ° C is not overcome (Fig. 35).

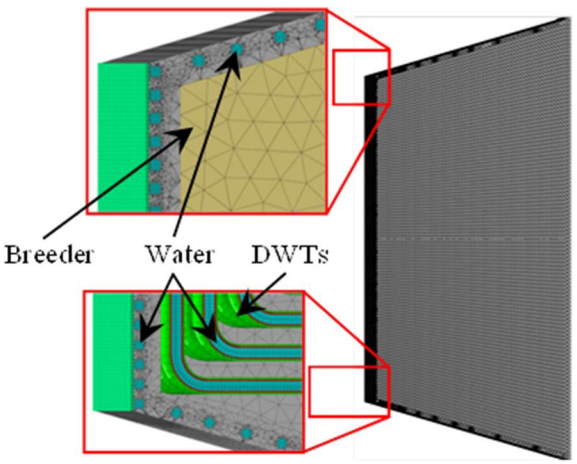

Fig. 34. Detailed 3D FEM model.

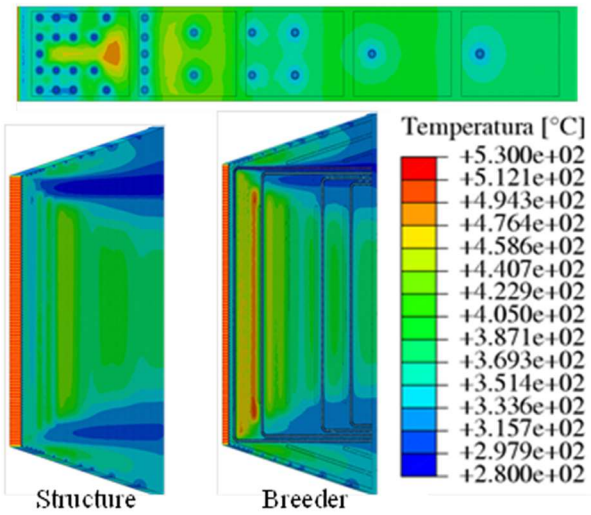

Fig. 35. Thermal field distribution - FW 4 configuration.

As to the mechanical behaviour, results have been processed performing stress linearization procedures in some critical paths of the FW (Fig. 36). Results show that the most critical paths are those located in the steel thickness between tungsten and channel, whatever is the toroidal height. Along these paths, the SDC-IC rule related to the immediate plastic flow localization results not verified both in the NO and in the OP loading scenarios. Table 7 reports a summary of the results of FW 4 configuration, obtained in the critical paths, located at two different toroidal heights. This configuration turns out to be the most promising to be considered for a conceptual design of the WCLL BB EOM.

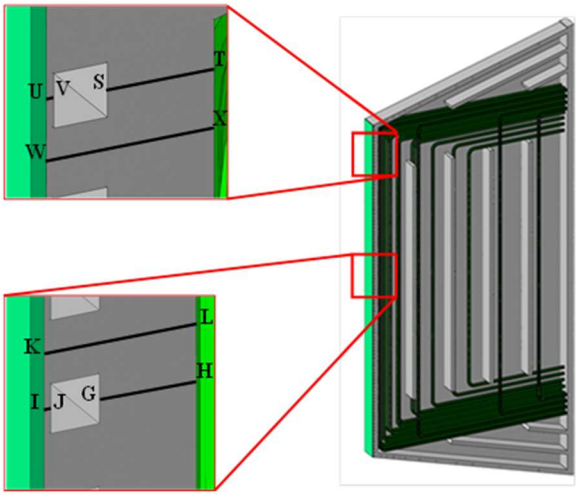

Fig. 36. Stress linearization paths at toroidal midplane.

Table 7. FW 4 configuration - Stress linearization results.

	Stress linearization path			
	CD	**IJ**	**OP**	**UV**
$T_{Max\text{-}Path}$ [°C]	447.9	449.34	423.2	425.0
Level A criteria				
P_m/S_m	0.066	0.087	0.093	0.098
$(P_m+P_b)/K_{eff}\ S_m$	0.052	0.064	0.063	0.066
$(P_m+Q_m)/S_e$	**1.036**	**1.059**	**2.028**	**2.140**
P_m/S_t	0.048	0.063	0.062	0.066
$(P_m+P_b/K)/S_t$	0.055	0.069	0.063	0.066
Level D criteria				
P_m/σ_{lim}	0.207	0.501	0.250	0.277
$(P_m+P_b)/K_{eff}\ \sigma_{lim}$	0.143	0.337	0.169	0.186
$(P_m+Q_m)/2\ S_e$	0.361	0.194	**1.102**	**1.158**
$W_t[1.35\ (P_m+P_b/K)]$	$2\cdot10^{-8}$	$4.3\cdot10^{-4}$	$4\cdot10^{-9}$	$1.4\cdot10^{-8}$

5.2 The SPs design

A parametric analysis campaign devoted to size the SPs has been performed. To this purpose a Stiffening Plates grid geometric layout foreseeing both radial-poloidal and radial-toroidal plates has been assumed, as an alternative to that previously considered in [20], in order to accomplish two main goals.

The first has been the reduction of the steel amount within the breeder zone, which affects the TBR, ensuring at the same time the Segment Box (SB) stiffness.

The second goal has been the possibility of basing the module design on a radial-toroidal elementary geometric cell repeated along poloidal direction, with the aim of improving the breeder circulation inside the module.

The SPs layout taken into account foresees radial-poloidal (rp) plates together with, on the radial-toroidal (rθ) plane, both pierced (rθ p) and filled (rθ) ones. In particular the former does not have structural function, being mainly devoted to opportunely address the breeder flow inside the module.

In order to size the SPs, the potential influence on their thermo-mechanical behaviour, which is reflected on the SB stiffness, of their number (N) and thickness (S) has been assessed, under conservative steady state loading conditions consisting in an uniform temperature equal to 550 ° C and a uniform internal pressure of 15.5 MPa, on both water and breeder wetted surfaces, intended to simulate an in-box LOCA accident.

Assuming reasonable and physically meaningful values for N and S of rp, pierced and filled rθ SPs, 14 different SPs geometric configurations have been assessed (Tab. 8). It has to be noted that in some configurations, radial-toroidal ribs (ri) and/or radial-toroidal kerbs (ke) have been also considered (Fig. 37) in addition to the afore mentioned SPs.

For each SPs configuration assessed, a proper 3D FEM model, reproducing the wavy SB already adopted in [2] properly endowed with a potentially optimized SPs configuration, has been set-up.

Table 8. Summary of the SPs configurations investigated.

Case	N_{rp}	S_{rp}[m]	$N_{r\theta\ p}$	$S_{r\theta\ p}$[m]	$N_{r\theta}$	$S_{r\theta}$[m]
0	0	-	3	0.002 - 0.02	0	-
1	5	0.016	4	0.002	3	0.016
2	5	0.016	4	0.010	3	0.016
3	5	0.016	6	0.002	5	0.016
3-1	5	0.016	4 ri	0.010	5	0.016
3-2	5	0.016	4 ri	0.020	5	0.016
3-3	5	0.016	4+8 ri	0.002 + 0.01	5	0.016
3-4	5	0.016	4ke+8ri	0.002	5	0.016
3-5	5	0.016	4	0.002	5	0.016
4	5	0.016	4	0.002	3	0.020
5	5	0.016	5	0.002	4	0.012
6	5	0.016	9	0.002	10	0.008
7	5	0.016	9	0.002	10	0.012
8	10	0.012	9	0.002	10	0.012

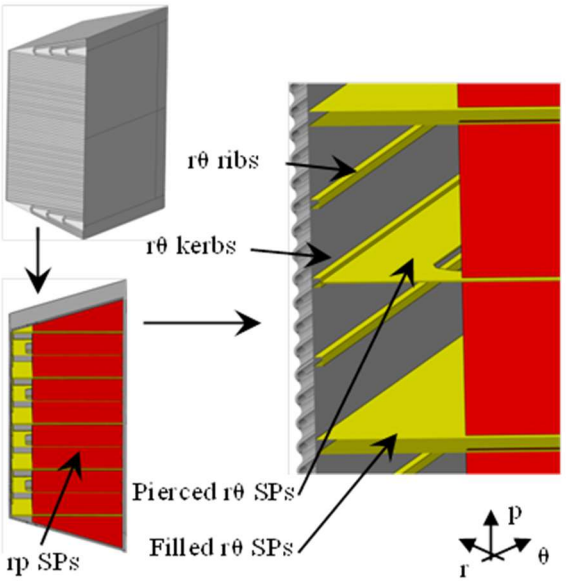

Fig. 37. Case 3-4 of the SPs parametric campaign.

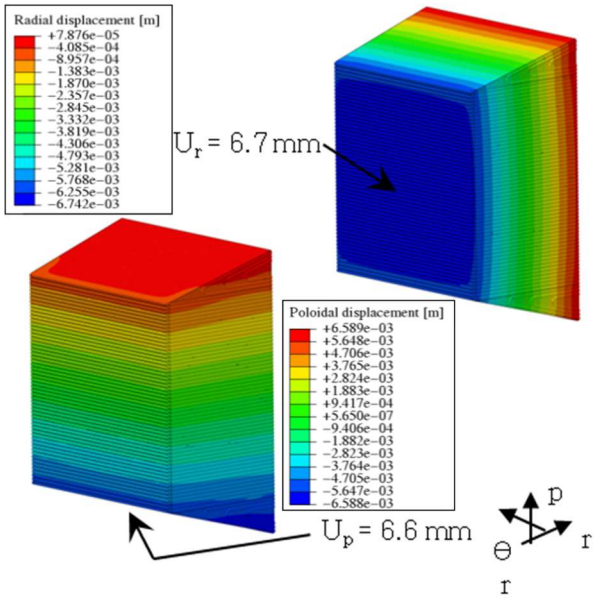

Fig. 38. Displacement fields of SB endowed with Case 8 SPs.

For each 3D FEM model set-up, un-coupled steady state thermo-mechanical analysis, under the afore mentioned conservative steady state loading conditions, has been performed.
Results in terms of SB radial and poloidal maximum displacements (max u_r and max u_p) have been assessed in order to select the SPs configuration able to make stiffer the SB under the severe accidental conditions assumed. Results have shown that Case 8 SPs are the most encouraging among those investigated. In fact, for the SB endowed with this SPs configuration, a maximum u_p of 6.6 mm and a maximum u_r of 6.7 mm have been predicted (Fig. 38). Qualitatively, similar outcomes have been found for Case 7 (max u_p = 7.1 mm and max u_r = 6.9 mm). These displacements values have been considered as acceptable if compared with those obtained in [2], therefore Case 7 or Case 8 SPs should be considered for the design of the WCLL BB outboard equatorial module. It has to be noted that a stiffening grid design according to Case 7 features consists of a reduced steel volume in comparison with Case 8. For this reason Case 7 might be preferred in order to design the outboard equatorial module without excessively affect its TBR.

5.3 Thermo-mechanical analysis of WCLL EOM

The development of WCLL EOM is based on the outcomes of the FW and SPs parametric optimization. Thermo-mechanical performances under the updated NO and OP steady state loading scenarios have been investigated, in accordance with SDC-IC structural design code. To this purpose, a realistic 3D FEM model of the whole WCLL BB outboard segment, representing the equatorial module directly tied to the BSS and the other outboard segment "dummy" modules, has been set-up (Fig. 39).

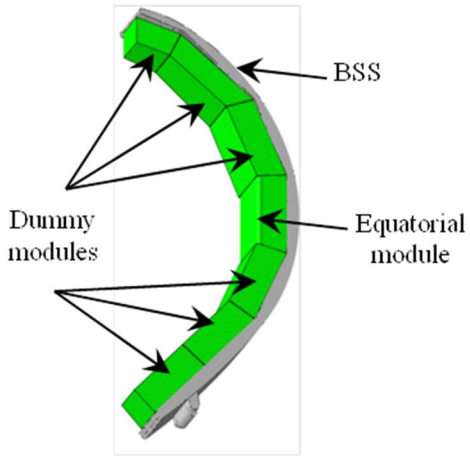

Fig. 39. 3D FEM model of the WCLL BB outboard segment.

From the thermal point of view, two different loading conditions have been taken into account, differing each other in the heat flux value applied on the FW plasma-facing surface. The first, named Case 1, has foreseen a maximum value of 0.5 MW/m² imposed onto the straight surface of the FW, while in the second, named Case 2, a maximum value of 1.4 MW/m² has been imposed onto the same surface. Concerning the bend FW surfaces, a cosine-dependent law has been adopted for them.

A proper non-uniform spatial distribution of heat power volumetric density has been applied to the model to simulate the deposited nuclear power density.

Forced convective heat transfer between structure and coolant has been simulated modelling convective heat transfer within water domain with a simplified FEM approach and adopting a proper thermal contact model between the coolant and the structure wetted walls [20].

As far as dummy modules are concerned, a non-uniform thermal field linearly depending on the radial distance from the FW has been imposed to them. In particular, temperature values ranging from 500 °C on the FW to 300 °C on the BP have been foreseen. This spatial distribution of temperature has been drawn from preliminary analyses performed on the WCLL outboard equatorial module [12]. As to BSS, a uniform temperature of 350 °C has been assumed.

From the mechanical point of view two different loading conditions have been taken into account for each thermal case, according to the scenario considered. Regarding the NO loading scenario, the mechanical effect of the water coolant flowing into FW, SW and cap channels, as well as DWTs has been reproduced imposing a pressure of 15.5 MPa to all water-wetted surfaces. A pressure of 0.5 MPa has been foreseen for the breeder-wetted surfaces. As far as the OP loading scenario is concerned, a pressure of 18.6 MPa, equal to the coolant pressure increased by 20%, has been imposed onto all wetted surfaces in order to take into account a coolant leak inside the box.

Moreover, the thermal deformation field arising within the model as a consequence of its non-uniform temperature distribution and its isotropic thermal expansion tensor has been considered in both the loading scenarios investigated. Finally, the weight force has been applied to the whole model.

Concerning mechanical restraints, a simplified set of mechanical boundary conditions has been imposed to nodes lying onto the BSS rear surface in order to simulate the attachment system devoted to connect BSS to the Vacuum Vessel.

Un-coupled steady state analysis have been run and thermal results have shown that temperature values remain below the EUROFER maximum allowable value of 550 °C except in Case 2, where the temperature reaches the maximum value of 582 °C in very restricted areas located near the Cap corners (Fig. 40).

As far as mechanical results are concerned, a stress linearization procedure has been carried out along some significant paths of the SB in order to verify whether the Level A and Level D safety criteria are fulfilled. In particular, paths lying on the toroidal mid-plane have taken into account for FW and BP (Fig. 41), while paths lying on different poloidal and radial planes have been considered for the SPs (Fig. 42).

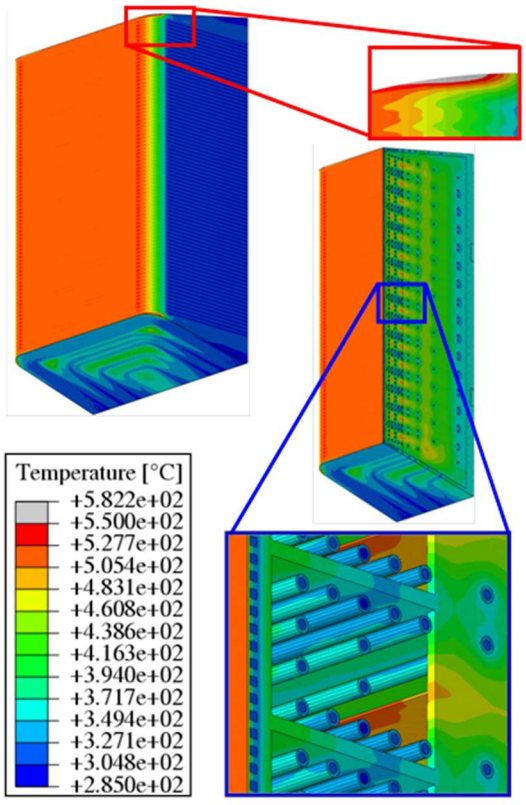

Fig. 40. Case 2 thermal results.

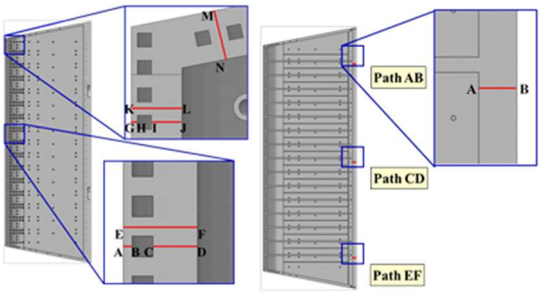

Fig. 41. FW and BP paths at toroidal mid-plane.

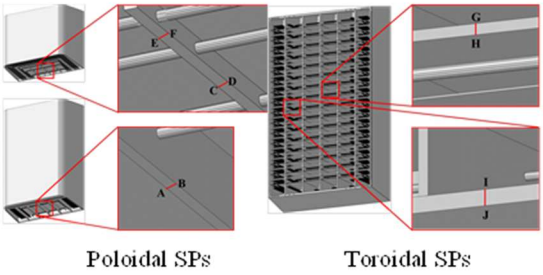

Fig. 42. Paths located within SPs.

Mechanical results relevant to NO scenario have shown, for both Case 1 and Case 2, that the most critical areas are those related to paths located within the SPs and near the Cap, where the criterion against plastic flow localization is not fulfilled. This is probably due to the resistance exerted by vertical SPs against the thermal expansion of horizontal SPs and vice versa, as well as to the compression exerted by BP and Caps, due to their lower poloidal thermal expansion with respect to FW, for paths located near the Cap (Tab. 9).

Table 9. SDC-IC safety criteria in most critical paths.

Case 1	**Stress linearization path**			
	FW_{GH}		**FW_{GH}**	
$T_{Max\text{-}Path}$ [°C]	407.7	$T_{Max\text{-}Path}$	407.7	$T_{Max\text{-}Path}$
Level A criteria		**Level A**		**Level A**
P_m/S_m	0.074	P_m/S_m	0.074	P_m/S_m
$(P_m+P_b)/K_{eff}\ S_m$	0.070	(P_m+P_b)	0.070	(P_m+P_b)
$(P_m+Q_m)/S_e$	**2.030**	$(P_m+Q_m$	**2.030**	$(P_m+Q_m$
Level D criteria		**Level D**		**Level D**
P_m/σ_{lim}	0.676	P_m/σ_{lim}	0.676	P_m/σ_{lim}
$(P_m+P_b)/K_{eff}\ \sigma_{lim}$	0.616	(P_m+P_b)	0.616	(P_m+P_b)
$(P_m+Q_m)/2\ S_e$	**1.690**	$(P_m+Q_m$	**1.690**	$(P_m+Q_m$
$W_t[1.35\ (P_m+P_b/K)]$	-	$W_t[1.35$	-	$W_t[1.35$

Case 2	**Stress linearization path**			
	FW_{GH}		**FW_{GH}**	
$T_{Max\text{-}Path}$ [°C]	520.6	$T_{Max\text{-}Path}$	520.6	$T_{Max\text{-}Path}$
Level A criteria		**Level A**		**Level A**
P_m/S_m	0.090	P_m/S_m	0.090	P_m/S_m
$(P_m+P_b)/K_{eff}\ S_m$	0.084	(P_m+P_b)	0.084	(P_m+P_b)
$(P_m+Q_m)/S_e$	**3.640**	$(P_m+Q_m$	**3.640**	$(P_m+Q_m$
Level D criteria		**Level D**		**Level D**
P_m/σ_{lim}	0.832	P_m/σ_{lim}	0.832	P_m/σ_{lim}
$(P_m+P_b)/K_{eff}\ \sigma_{lim}$	0.784	(P_m+P_b)	0.784	(P_m+P_b)
$(P_m+Q_m)/2\ S_e$	**2.680**	$(P_m+Q_m$	**2.680**	$(P_m+Q_m$
$W_t[1.35\ (P_m+P_b/K)]$	**2.470**	$W_t[1.35$	**2.470**	$W_t[1.35$

Concerning the OP loading scenario, paths located near the Cap continue to do not satisfy all safety criteria, especially in Case 2 where the high temperatures reached on the FW cause the failure also for creep damage. On the other hand, less SP paths fail to fulfil the criteria, probably due to the effect of the higher pressure imposed on the internal SB surfaces. All paths located within the BP successfully fulfil all safety criteria in all loading scenarios investigated.

In conclusion, results obtained in both cases show that a revision of the SPs has to be performed in order to limit their secondary stresses, by possibly changing their thickness and number, as well as to reinforce the FW top and bottom corner regions to avoid their failure due to immediate plastic flow localisation. Moreover, since results appear to be dependent on the BSS displacement, a more accurate simulation of the attachment system devoted to connect BSS to Vacuum Vessel is needed.

6. Integration with PHTS

The main function of the PHTS is to provide cooling water to the first wall and blanket modules and to transfer the thermal power to the power conversion system (PCS). FW and BZ cooling systems are separated, thus from the upper port, two pipes enter to fed the segment, and two pipes exit to deliver the hot coolant to the PHTS. The overall primary system coolant mass flow rate is 10561 kg/s, calculated considering an inlet temperature of 295 °C, outlet temperature 328 °C, at 15.5 MPa, which is the new reference thermal-cycle. EUROFER pipeline dimensions are calculated

according with the velocity limit of 7 m/s. On the opposite, main pipeline diameters outside the vacuum vessel are calculated accounting for coolant velocity of 15 m/s, with a maximum limit of 20 m/s.

The BZ PHTS has two loops and deliver the power to the turbine by means of two Once Through Steam Generators (OTSG) during the pulse operation of DEMO. The FW PHTS exchange the heat with the energy storage system, using molten salt as fluid. This system is in charge to deliver the heat and to produce the electricity during the dwell time. Fig. 43 and Fig. 44 show the tokamak building, the two OTSGs, the pressurizer (PRZ) and the Intermediate Heat Exchanger (IHX) water-molten salt.

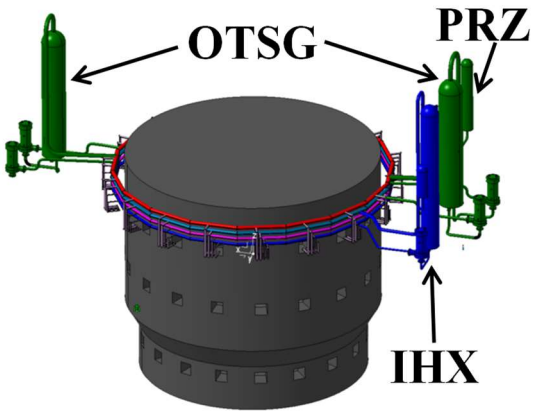

Fig. 43. Tokamak reactor and WCLL PHTS

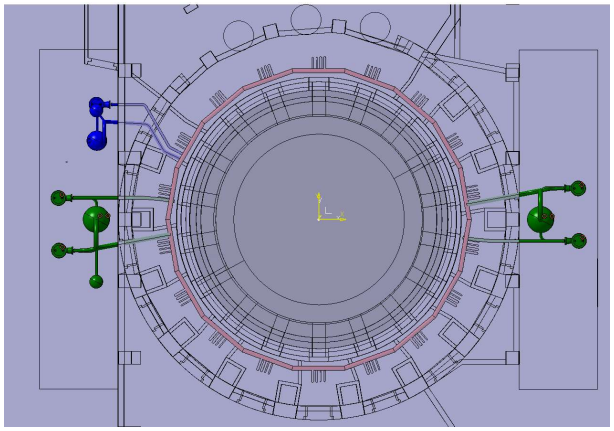

Fig. 44. Top view of WCLL PHTS

The cooling water is distributed and collected by means of four ring headers, hosted in a proper corridor 7x7 m that runs all around the tokamak (Fig. 45). The header diameter is DN650 for breeding cooling loop, and DN500 for first wall cooling loop. The primary coolant is pressurized by means of a pressurizer connected to the hot leg upstream of the steam generator. The type and location of this pressurizer were selected based on space considerations, pressure controllability, and safety criteria. The location of the main PHTS components with respect the tokamak building can be seen in Fig.46.

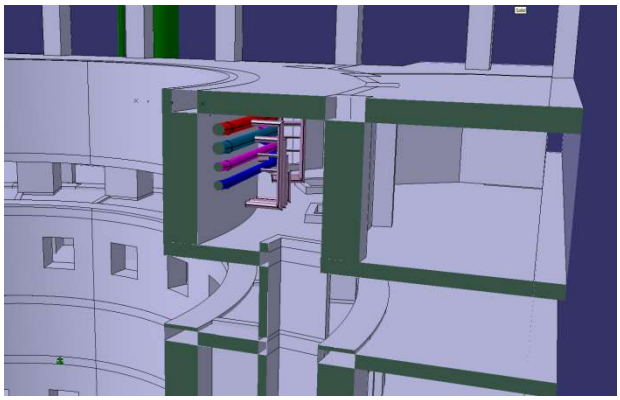

Fig. 45. Water distributors

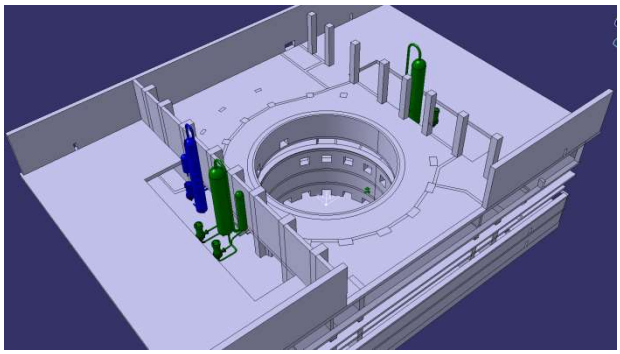

Fig.46. Displacement of PHTS in the tokamak building

4. Conclusions

The paper describes the current status of Water cooled lithium-lead breeding blanket conceptual design, presenting the single module configuration. The CAD model of WCLL BB inboard and outboard segment is available, including the BSS, manifolds and the integration with the PHTS. Detailed analyses have been performed to support design choices, and to demonstrate the reliability of the design. The main outcomes from the analyses are:

- Neutronics analyses, based on WCLL BB multi-module configuration, demonstrate that tritium self-sufficiency

design target and shielding requirements are fulfilled.

- Thermo-hydraulic analyses provided the temperature field in the domains and indicated the recirculation of coolant in the BZ tubes as promising solution to avoid toroidal asymmetry of PbLi and stiffeners temperature.
- Thermal analyses of inboard and outboard BSS demonstrate that the temperature is below the limit (550 °C), considering the inboard front wall cooled with water.
- The pressure drop due to MHD effects in the WCLL elementary cell is estimated equal to $2.06 \cdot 10^3$ Pa. Preliminary studies demonstrated that 3D MHD effects due to the cross-section variations do not contribute significantly to the cell pressure drop.
- Thermo-mechanical analyses demonstrate that the equatorial outboard module has the capability to fulfil the requirements prescribed by safety codes in NO and OP conditions, with few exceptions.

Acknowledgments

This work has been carried out within the framework of the EUROfusion Consortium and has received funding from the Euratom research and training programme 2014-2018 under grant agreement No 633053. The views and opinions expressed herein do not necessarily reflect those of the European Commission.

References

[1] F. Romanelli et al., Fusion Electricity – A roadmap to the realization of fusion energy, EFDA (Nov., 2012), pp. 20–28 ISBN 978-3-00-0407.

[2] L.V. Boccaccini, et al., Objectives and status of EUROfusion DEMO blanket studies, Fusion Eng. Des.109-111 (2016) 1199-1206.

[3] G. Federici, et al., Overview of the design approach and prioritization of R&D activities towards an EU DEMO, Fusion Eng. Des. 109-111 (2016) 1464–1474.

[4] A. Del Nevo, et al., WCLL breeding blanket design and integration for DEMO 2015: status and perspectives, Fusion Eng. Des. (2017), in press.

[5] R. Mozzillo, et al. Development of a master model concept for DEMO vacuum vessel. Fusion Engineering and Design, 2016, 112: 497-504.

[6] X-5 Monte Carlo Team: MCNP - A General Monte Carlo N-Particle Transport Code, Version 5, Los Alamos National Laboratory, Los Alamos, New Mexico, USA, April 2003

[7] JEFF-3.2 Evaluated Data Library—Neutron Data, OECD-NEA (2014), https://www.oecdnea.org/dbforms/data/eva/evatapes/jeff 32/

[8] U. Fischer, Guidelines for Neutronic Analyses, EFDA_D_2L8TR9

[9] U. Fischer, C. Bachmann, J.-C. Jaboulay, F. Moro, I. Palermo, P. Pereslavtsev and R. Villari, Neutronic Performance Issues of the Breeding Blanket Options for the European DEMO fusion power plant, Fus. Eng. Des., Vol. 109-111, Part B, pp 1458-1463, 2016

[10] www.spaceclaim.com

[11] Y. Wu, FDS Team, CAD-based interface programs for fusion neutron transport simulation, Fus. Eng. Des. 84 (2009) 1987 – 1992

[12] P. A. Di Maio, P. Arena, G. Bongiovì, P. Chiovaro, A. Del Nevo, R. Forte, Optimization of the breeder zone cooling tubes of the DEMO Water-Cooled Lithium Lead breeding blanket, Fusion Engineering and Design, 109-111 (2016), pp. 227-231.

[13] S. Smolentsev, R. Moreau, L. Buhler and C. Mistrangelo, "MHD thermofluid issues of liquid-metal blankets: phenomena and advances," Fusion Engineering and Design, 85(7), (2010), pp. 1196-1205.

[14] S. Smolentsev et al., "An approach to verification and validation of MHD codes for fusion applications," Fusion Engineering and Design, 100, (2015), pp. 65-72.

[15] I. Di Piazza & L. Buhler, "A general computational approach for magnetohydrodynamic flows using the CFX code: buoyant flow through a vertical square channel," Fusion Science and

Technology, 38(2), (2000), pp. 180-189.
[16] E. M. de les Valls et al., "Lead-lithium eutectic material database for nuclear fusion technology," Journal of Nuclear Materials, 376(3), (2008), pp. 353-357.
[17] K. Mergia & N. Boukos, "Structural, thermal, electrical and magnetic properties of Eurofer 97 steel," Journal of Nuclear Materials, 373(1), (2008), pp. 1-8.
[18] M. S. Tillack et al., "The effect of magnetic field alignment on heat transfer in liquid metal blanket channels," in IEEE Thirteenth Symposium on Fusion Engineering, 1989.
[19] P. A. Di Maio, P. Arena, J. Aubert, G. Bongiovì, P. Chiovaro, R. Giammusso, A. Li Puma, A. Tincani, Analysis of the thermo-mechanical behaviour of the DEMO Water-Cooled Lithium Lead breeding blanket module under normal operation steady state conditions, Fusion Engineering and Design, 98-99 (2015), pp. 1737-1740.
[20] P. Chiovaro, P. Arena, J. Aubert, G. Bongiovì, P. A. Di Maio, R. Giammusso, A. Li Puma, Assessment of the Thermo-mechanical Performances of a DEMO Water-Cooled Liquid Metal Blanket Module, Journal of Fusion Energy, 34 (2015), pp. 277-292.
[21] P. A. Di Maio, P. Arena, G. Bongiovì, P. Chiovaro, R. Forte, S. Garitta, On the optimization of the first wall of the DEMO water-cooled lithium lead outboard breeding blanket equatorial module, Fusion Engineering and Design, 109-111 (2016), pp. 335-341.
[22] ITER structural design criteria for in-vessel components (SDC-IC) code.
[23] F. Tavassoli, Fusion Demo Interim Structural Design Criteria (DISDC)/Appendix A Material Design Limit Data/A3.S18E Eurofer Steel, EFDA TASK TW4-TTMS-005-D01. CEA Report DMN/DIR/NT/2004-02/A, December 2004.